第35卷 第2期 焊 接 学 报 Vol. 35 No. 2
2014年2月 TRANSACTIONS OF THE CHINA WELDING INSTITUTION February 2014

超声冲击处理提高超音速等离子喷涂 Cr_3C_2-NiCr涂层性能

陈 健[1]， 吕 林[2]， 崔 庭[3]， 马万斌[1]， 史和生[2]
(1. 江苏科技大学 先进焊接技术省级重点实验室，镇江 212003;
2. 南京润邦金属复合材料有限公司，南京 211803; 3. 常州豪爵铃木摩托有限公司，常州 213022)

摘 要: Cr_3C_2-NiCr涂层是中高温下理想的耐磨、抗氧化、耐蚀涂层，常用于高温下的燃气冲蚀磨损、磨粒磨损、微动磨损、硬表面磨损等场合. 文中采用超音速等离子喷涂的方法在CuCrZr合金表面制备Cr_3C_2-NiCr涂层，并采用超声冲击的方法对涂层进行后处理. 结果表明，经超声冲击处理后，涂层孔隙率由2.34%降低至1.83%; 涂层的平均显微硬度由8.9 GPa提高至9.6 GPa，且硬度分布更均匀; 在650 ℃下进行热震试验，涂层的热震寿命显著提高，热震裂纹的扩展路径也发生了变化.

关键词: 超声冲击处理; 超音速等离子喷涂; Cr_3C_2-NiCr涂层; 涂层性能
中图分类号: TG174.442 **文献标识码:** A **文章编号:** 0253-360X(2014)02-0095-04

0 序 言

热喷涂涂层的性能主要由涂层扁平粒子的层间结合和扁平粒子内部的组织结构所决定，而粒子与基体发生碰撞后的扁平化过程主要受粒子撞击速度、熔化状态等因素的制约，于是提高热喷涂射流和粒子的速度成为当今国内外热喷涂技术发展的新趋势，相继出现了超音速火焰喷涂、高速电弧喷涂、气体爆炸喷涂及超音速等离子喷涂技术[1]. 超音速等离子喷涂的主要优点是利用超音速等离子体射流，将熔融粒子加速至音速以上(400~1 000 m/s)[2]. 因其粒子飞行的速度远大于普通等离子喷涂，故形成的涂层致密性和结合强度均显著提高. 采用合适的打底层形成复合涂层或对涂层进行适当的后处理也是提高涂层性能的有效措施[3]. 在后处理方面，主要方法有: 激光重熔、激光"钉扎"、扩散热处理、超声深滚法[4,5]等.

CuCrZr合金作为连铸生产中结晶器材料之一，其承受着高温氧化、冷热疲劳应力、化学腐蚀，摩擦磨损等伤害，工作状况恶劣. CuCrZr合金表面必须采取相应的保护措施. 文中用超音速等离子喷涂法在CuCrZr合金表面制备Cr_3C_2-NiCr涂层，并用超声冲击处理(ultrasonic impact treatment, UIT)方法对涂层进行后处理，研究冲击处理对涂层性能的影响.

收稿日期: 2012-11-08
基金项目: 江苏高校优势学科建设工程资助项目

1 试验方法

基体材料为CuCrZr合金，长宽高尺寸为40 mm×40 mm×5 mm，表面喷砂处理后进行超音速等离子喷涂. 涂层粉末为北京矿冶研究总院金属材料研究所生产的烧结型Cr_3C_2-30NiCr粉末. 喷涂设备为美国Praxair公司生产的3710型等离子喷涂系统，喷枪为SG-100型等离子喷枪. 喷涂工艺参数如下: 喷涂距离120 mm，主气流量64.9 L/min，送粉速率25 g/min，功率60 kW. 超声冲击设备为自行研制，振动频率20 kHz(图1a)，有多种类型的枪头可供选择(图1b)，文中采用图1b中间的球冠枪头，每根针头直径2 mm.

用JSM-6480型扫描电镜观察涂层截面的显微形貌，用专业软件分析涂层截面的孔隙率，用MH-5型显微硬度计测量涂层截面的显微硬度. 热震试验采用SX2-10-12型箱式电阻炉，过程为: 将四块试样放入电阻炉内加热到650 ℃，保温10 min，然后取出并迅速投入25 ℃±5 ℃水中淬冷，观察涂层是否发生开裂及脱落，如涂层完好，则继续放入电阻炉内保温，如此循环，直到四块试样中任意一块出现裂纹，记录该试样总的热震循环次数即为试样的宏观启裂次数.

2 试验结果与分析

2.1 超声冲击处理对涂层显微组织结构的影响

图2和图3分别为超声冲击处理前后Cr_3C_2-

(a) 超声冲击枪及电源

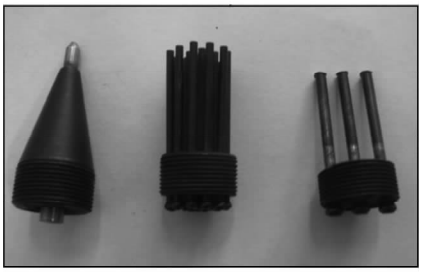

(b) 冲击枪头

图 1 超声冲击设备

Fig. 1 Ultrasonic impact treatment equipment

NiCr 涂层截面的显微形貌. 其中,深色颗粒为 Cr_3C_2 硬质相,其余的灰色区域为 NiCr 粘结相. 从图 2a,b 可以看出: 在基体与涂层的界面处及靠近界面的涂层中均存在较多的空隙和疏松,其它区域的空隙和疏松则有所降低,经测量其平均孔隙率为 2.34%; 从图 3a,b 可以看出: 超声冲击处理后,无论是基体与涂层的界面区域还是其它区域的空隙和疏松都有明显减少,经测量其平均孔隙率为 1.83%,且涂层

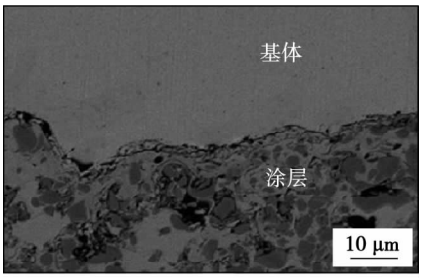

(a) 界面区

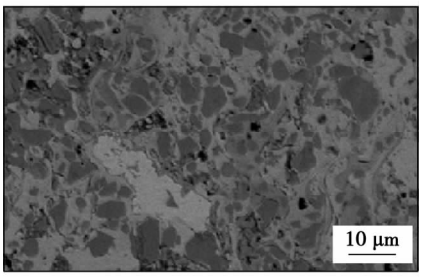

(b) 涂层截面

图 2 未经超声冲击的 C_3C_2-NiCr 涂层截面显微形貌

Fig. 2 Microscopic morphology of Cr_3C_2-NiCr coating before ultrasonic impacting

组织更均匀. 这是因为 Cr_3C_2-NiCr 涂层是由 Cr_3C_2 硬质颗粒外面包覆着 NiCr 合金经变形层叠而成,而 NiCr 合金具有一定的塑性,进行超声冲击处理时涂层材料的剧烈塑性变形导致晶粒细化、孔隙闭合、致密性提高、涂层与基体间的结合程度更加紧密.

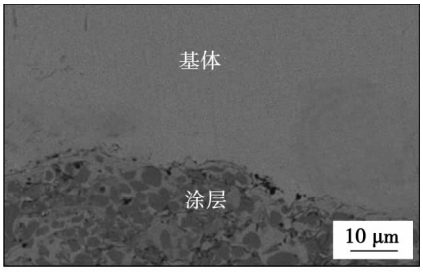

(a) 界面区

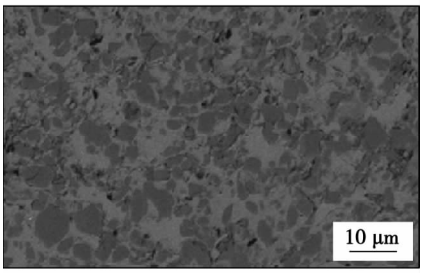

(b) 涂层截面

图 3 超声冲击后 Cr_3C_2-NiCr 涂层截面显微形貌

Fig. 3 Microscopic morphology of Cr_3C_2-NiCr coating after ultrasonic impacting

2.2 超声冲击处理对涂层显微硬度的影响

硬度是表征涂层耐磨性和强度的最接近的性能参数. 一些孔隙(或裂纹)和一定数量的未熔颗粒造成的疏松等,使涂层局部区域的硬度降低,因此,涂层的硬度存在较大的分散性,但通常符合正态分布[8],为此,在超声冲击前后的涂层截面上各随机选取 50 个位置测量显微硬度,对硬度进行统计分析. 图 4a 为超声冲击处理前涂层显微硬度分布柱状图,95% 置信区间为(8.2 GPa,9.6 GPa),5% 修整均值为 8.9 GPa. 图 4b 为超声冲击处理后涂层显微硬度分布柱状图,95% 置信区间为(8.8 GPa,10.5 GPa),5% 修整均值为 9.6 GPa. 可见,超声冲击处理后涂层显微硬度的分布与正态分布曲线拟合度更好,平均显微硬度也由冲击前的 8.9 GPa 提高到冲击后的 9.6 GPa. 说明超声冲击处理不仅可以提高硬度,而且还可以提高涂层硬度的均匀性. 原因在于超声冲击处理使涂层中的 NiCr 相产生塑性流变,使得晶粒细化、空隙减少和产生加工硬化作用所致.

2.3 超声冲击处理对涂层热震性能的影响

在 650 ℃的热震试验条件下,未经超声冲击处

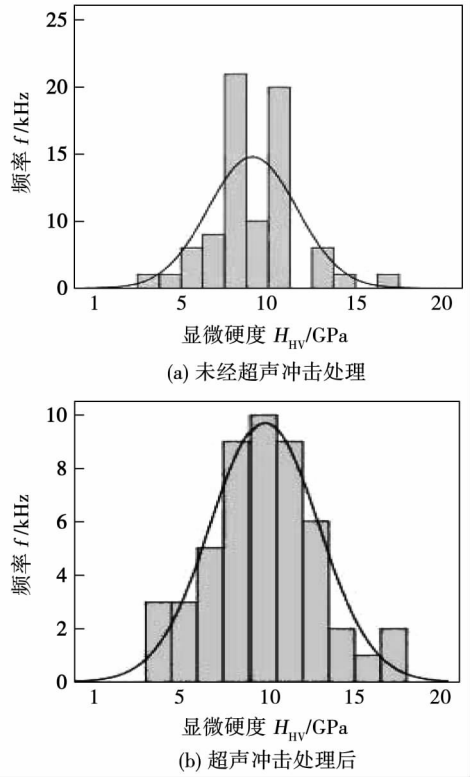

图 4　Cr_3C_2-NiCr 涂层显微硬度分布柱形图

Fig. 4　Micro-hardness distribution bar diagram of Cr_3C_2-NiCr coating

理的涂层的宏观启裂次数为 7 次,经超声冲击处理后,涂层的宏观启裂次数增加至 11 次,涂层的热震寿命大幅提高.

图 5 为试样经热震后涂层开裂的宏观形貌. 热震裂纹均产生于试样边缘的涂层与基体的界面处并沿界面向纵深扩展,但两者的扩展路径并不相同. 对于未经超声冲击处理的涂层,热震裂纹在试样边缘产生后沿界面向试样中心扩展(图 5a),最终当不同方向的裂纹相遇后,导致涂层发生整体剥落. 对涂层进行超声冲击处理后再进行热震试验,裂纹形成后并不向试样中心扩展,而是向相邻的边缘扩展(图 5b),裂纹不易相交,延缓了涂层的整体脱落.

涂层在热震条件下的失效,本质上是在循环应力作用下的疲劳失效,主要取决于涂层中热应力的大小和涂层的结合强度[7]. 在加热阶段,涂层主要受拉应力,基材受压应力,拉应力导致涂层内部产生裂纹和开裂[8,9],但涂层内本身存在的残余应力也会对涂层的热震性能产生影响,且残余应力在涂层的表面主要亦为拉应力,因此,热震试验时,涂层中的残余拉应力与热应力引起的拉应力相互叠加交互作用,使涂层热震疲劳寿命大幅下降.

经超声冲击处理后,涂层会在垂直于基体方向

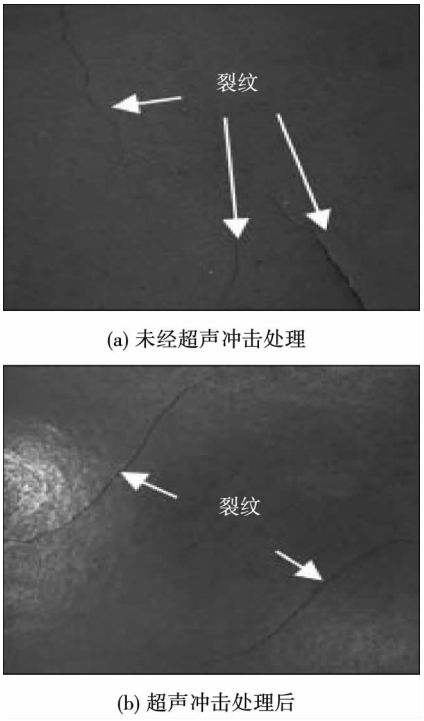

图 5　Cr_3C_2-NiCr 涂层热震后开裂形貌

Fig. 5　Surface appearance of Cr_3C_2-NiCr coatings thermal shock specimen

产生一定的压缩塑性变形,同时也会在平行于基体方向产生一定的塑性延展,因而可以改善涂层中残余应力的分布,降低涂层中的残余拉应力,甚至使涂层中残余应力由冲击前的拉应力转变为压应力,从而在一定程度上阻碍了热震裂纹的产生与扩展并使扩展路径发生相应的变化; 此外,塑性变形,提高了涂层的致密度,改善了涂层的组织结构,亦可提高涂层的热疲劳寿命.

3　结　　论

(1) 超声冲击处理降低了 Cr_3C_2-NiCr 涂层的孔隙率,孔隙率由冲击前的 2.34% 降低至 1.83%.

(2) 超声冲击处理后,Cr_3C_2-NiCr 涂层的显微硬度有所提高,平均显微硬度由冲击前的 8.9 GPa 提高至 9.6 GPa.

(3) 650 ℃下进行热震试验,Cr_3C_2-NiCr 涂层的宏观启裂次数由冲击前的 7 次提高至 11 次,冲击还改变了热震裂纹的扩展路径.

参考文献:

[1]　王海军, 谢兆钱, 郭永明, 等. 高效能超音速等离子喷涂粒子特性及涂层特点[J]. 中国表面工程, 2010, 23(3): 84-88.

Wang Haijun, Xie Zhaoqian, Guo Yongming, *et al*. Characteristic of high efficiency supersonic plasma spraying particles and coatings [J]. China Surface Engineering, 2010, 23(3): 84 – 88.

[2] 陈 健, 刘雪飘, 梁 欢, 等. CuCrZr 合金表面等离子喷涂 Cr_3C_2–NiCr 及 NiAl/Cr_3C_2–NiCr 涂层的结合性能 [J]. 焊接学报, 2012, 33(5): 13 – 16.
Chen Jian, Liu Xuepiao, Liang Huan, *et al*. Bonding properties of plasma sprayed Cr_3C_2–NiCr and NiAl/Cr_3C_2–NiCr coatings on Cu–CrZr alloy surface [J]. Transactions of the China Welding Institution, 2012, 33(5): 13 – 16.

[3] 陈 健, 刘雪飘, 梁 欢. 铜及铜合金表面等离子喷涂的应用进展 [J]. 金属热处理, 2010, 35(9): 98 – 103.
Chen Jian, Liu Xuepiao, Liang Huan. Research progress and application of plasma spraying on copper alloy surface [J]. Heat Treatment of Metals, 2010, 35(9): 98 – 103.

[4] 黄元林, 朱有利, 彭艳杰. 超声深滚法提高电弧喷涂 3Cr13 涂层性能 [J]. 机械工程学报, 2010, 46(6): 107 – 110.
Huang Yuanlin, Zhu Youli, Peng Yanjie. Improvement of the properties of electric arc spray 3Crl3 coating by ultrasonic deep rolling method [J]. Journal of Mechanical Engineering, 2010, 46(6): 107 – 110.

[5] Xu Binshi, Wang Haidou, Dong Shiyun, *et al*. Transactions of materials and heat treatment [J]. Nano Surface Engineering in the 21th Century, 2004, 25(5): 8 – 12.

[6] 陈 健, 崔 庭. CuNiCoBe 合金表面等离子喷涂 Cr_3C_2–NiCr 涂层 [J]. 焊接技术, 2012, 41(5): 17 – 20.
Chen Jian, Cui Ting. Plasma spraying Cr_3C_2–NiCr coating on Cu–NiCoBe alloy surface [J]. Welding Technology, 2012, 41(5): 17 – 20.

[7] 向兴华, 全成军, 朱景川, 等. 钛合金表面等离子喷涂 ZrO_2–NiCoCrAlY 梯度涂层的抗热震行为 [J]. 宇航学报, 1998, 19(2): 61 – 65.
Xiang Xinghua, Quan Chengjun, Zhu Jingchuan, *et al*. Thermal shock behaviour of plasma sprayed ZrO_2 NiCoCrAlY graded coating on Ti-6Al-4V substrate [J]. Journal of Astronautics, 1998, 19(2): 61 – 65.

[8] 苟国庆. 内燃机车气缸等离子喷涂修复技术研究 [D]. 成都: 西南交通大学, 2006.

[9] 沈金文, 吕广庶, 马 壮, 等. 在热震试验中热障涂层的裂纹形成和扩展 [J]. 新技术新工艺, 2002(4): 39 – 41.
Shen Jinwen, Lv Guangze, Ma Zhuang, *et al*. The cracks forming and developing of thermal barrier coating in thermal shock [J]. New Technology, 2002(4): 39 – 41.

作者简介: 陈 健,男,1963 年出生,副教授. 主要从事高性能铜合金的开发、焊接、等离子喷涂方面的科研和教学工作. Email: jsch168@yeah.net

通讯作者: 崔 庭,男,工程师. Email: more_fun@126.com

consumables, and the microstructure of the joints and the tensile strength of weld joints were studied. Results indicate that with the recommended welding parameters, the weld joints possessed high tensile strength with Al-Si welding wires, and the microstructure of the weld was as cast microstructure of dendrite, which was different with the cellular crystal of the fusion zone. The crystalline grain in the HAZ was slightly coarsened by the influence of the welding thermal cycles. The tensile strength and the tendency of forming large pores of the ER4043 weld joint was relatively lower than the ER4047 joint, but the ductility of joint welded with ER4043 was better.

Key words: marine aluminum alloy; TIG; microstructure; mechanical properties

Properties improvement of supersonic plasma spraying Cr_3C_2-NiCr coating by ultrasonic impact treatment

CHEN Jian[1], LV Lin[2], CUI Ting[3], MA Wanbin[1], SHI Hesheng[2] (1. Provicial Laboratory of Advanced Welding Technology, Jiangsu University of Science and Technology, Zhenjiang 212003, China; 2. Nan Jing Run Bang Clad Metal Material Co., Ltd, Nanjing 211803, China; 3. The Changzhou Haojue Suzuki Motorcycle Co., Ltd, Changzhou 213022, China). pp 95 - 98

Abstract: For the ideal resistance characteristics to wear, oxidation and corrosion, Cr_3C_2-NiCr coating has been widely used in the gas erosive wear, abrasive wear, fretting wear and hard surface wear under high temperature conditions. In this paper, Cr_3C_2-NiCr coating on CuCrZr was obtained by supersonic plasma-spraying method, and the post-processing ultrasonic impact treatment was utilized to certain coating. The results show that porosity of the coating decreases from 2.34 percent to 1.83 percent, and average micro-hardness of coating increases from 8.9 GPa to 9.6 GPa and hardness distribution becomes uniform. Coating thermal shock life at 650 ℃ improves markedly; meanwhile, crack path of thermal shock also changes.

Key words: ultrasonic impact treatment; supersonic plasma spraying; Cr_3C_2-NiCr coating; coating properties

Properties of Al-Mg alloys joints welded by refill friction stir spot weldeing process

WANG Lianfeng, ZHU Xiaogang, QIAO Fengbin, GUO Lijie (Shanghai Aerospace Equipments Manufacturer, Shanghai 200245, China). pp 99 - 103

Abstract: In order to determine the properties of refill friction stir spot welded (RFSSW) Al-Mg alloys joints, tests on tensile/shear strength, cross-tension strength, microstructure and fatigue properties of refill friction stir spot welded joints were conducted with 2mm-thickness 5A06 aluminum alloy as research subject, and microstructure model of RFSSW joint was established as well. Experimental results indicated that the microstructure of the joints could be divided into nugget zone, heat affected zone, thermo-mechanically affected zone and base material, respectively. When the rotational speed was 2 000 rpm, the tensile/shear strength was able to reach 8 194 N, and the highest cross-tension strength was 3565N. SEM and OM analysis showed that fatigue cracks initiated from weld edge on the joining surface of the upper and lower plates, and defects including ring groove, cavity, aluminum clad in this area, as well as stress concentration were the main causes for fatigue damage.

Key words: Al-Mg alloy; refill friction stir spot welding; properties

Engineering applications of MIG welding deformation simulation of aluminum alloy sheet

LI Xiaodong, LI Chunguang, ZHU Zhimin, XU Fenglin (CSR Nanjing Puzhen Co., Ltd., Nanjing 210031, China). pp 104 - 108

Abstract: It is a great challenge to control the welding deformation of aluminum alloy sheet because of its characteristics of both material and structure. This kind of deformation is a key problem of welding quality in the railway industry. In this paper, more attentions have paid to welding distortion of joints made of aluminum alloy sheet by MIG welding. Herein, numerical simulation was served as an effective tool for simulating welding deformation. Based on moving heat source model and sectional temperature function, the welding process of top slab of end wall with 2.2mm thickness was simulated. Results showed that range of error between the deformation values of simulation and actual measurement was within 20%, the morphology of the welding pool simulated was basically in agreement with the experimentally measured results. Backward deformation and simulated structure coincide well with the results of actual welding process, welding process optimization of top slab of end wall was carried out by controlling arm pressure and position, welding sequence and backward deformation method.

Key words: aluminum; body sheet; welding deformation; Simulation

Microstructure and properties of dissimilar materials Cu/Ti lapped joint by friction stir welding

YAO Lei[1], SHEN Yifu[1], LI Bo[1], HU Weiye[2] (1. College of Material Science and Technology, Nanjing university of Aeronautics and Astronautics, Nanjing 210016, China; 2. Technology Research Institute of Nanjing Chenguang Group Co., Ltd., China Aerospace Science and Industry Corporation, Nanjing 210012, China). pp 109 - 112

Abstract: The lap joint of commercial purity titanium (TA2) and copper (T2) plates were successfully produced via friction stir welding technique, the macrostructure and microstructure of Cu/Ti lap interface were researched respectively. The mechanical properties of the joint were characterized by tensile shear tests as well. The results show that the defect-free lap-welds with well-formed surface and interface of joint were obtained when rotation speed and travel speed were 800 r/min, 40 mm/min respectively. The interface of joint exhibited the typical bounded texture microstructure of Cu and Ti in the stir zone, and a region of swirling-like of bimetallic weld of TA2 titanium and T2 copper was formed. Moreover, mechanical interlock was formed in some parts of lap joint. A maximum failure load of 95% of the one of T2 copper was achieved, and the fracture location was located in the advancing side of copper, the fracture was the typical ductile fracture.

Key words: friction stir welding; lap; copper; titanium; bounded texture microstructure